



Burned Area Detection in the Brazilian Amazon using Spectral Indices and GEOBIA

Detecção de Áreas Queimadas na Amazônia Brasileira usando Índices Espectrais e GEOBIA

Thales Vaz Penha¹, Thales Sehn Körting², Leila Maria Garcia Fonseca³, Celso Henrique Leite Silva Junior⁴, Mikhaela Aloísia Jéssie Santos Pletsch⁵, Liana Oighenstein Anderson⁶ e Fabiano Morelli⁷

¹ University of São Paulo, Department of Physical Geography, São Paulo, Brazil. National Institute for Space Research, Image Processing Division, São José dos Campos, Brazil. thalesvazpenha@gmail.com; ORCID: <https://orcid.org/0000-0002-9560-4186>

² National Institute for Space Research, Image Processing Division, São José dos Campos, Brazil. thales.korting@inpe.br; ORCID: <https://orcid.org/0000-0002-0876-0501>

³ National Institute for Space Research, Image Processing Division, São José dos Campos, Brazil. leila.fonseca@inpe.br; ORCID: <https://orcid.org/0000-0001-6057-7387>

⁴ National Institute for Space Research, Remote Sensing Division, São José dos Campos, Brazil. celso.junior@inpe.br; ORCID: <https://orcid.org/0000-0002-1052-5551>

⁵ National Institute for Space Research, Image Processing Division, São José dos Campos, Brazil. mikhaela.pletsch@inpe.br; ORCID: <https://orcid.org/0000-0002-1690-1175>

⁶ National Center for Monitoring and Early Warning of Natural Disasters, São José dos Campos, Brazil. liana.anderson@cemaden.gov.br; ORCID: <https://orcid.org/0000-0001-9545-5136>

⁷ National Institute for Space Research, Earth Observation Coordination, São José dos Campos, Brazil. fabiano.morelli@inpe.br; ORCID: <https://orcid.org/0000-0003-2110-4477>

Recebido: 05.2019 | Aceito: 04.2020

Abstract: Mapping refined burned areas (BA) in the Brazilian Amazon is still a challenge. The main difficulty of BA detection in large areas is the presence of cloud cover and water bodies. The use of different data sources of medium spatial resolution satellite images can provide a higher availability of cloud-free images. Besides that, it may decrease the uncertainties associated with coarse spatial resolution data (>250m), which can under or overestimate BA and hinder the detection of small BA patches (<0.1km²). In this study, we propose an innovative methodology based on spectral indices and geographic object-based image analysis (GEOBIA), using medium spatial resolution images to improve BA detection in the Brazilian Amazon region. Firstly, we assessed the performance of nine spectral indices in two study areas, derived from Landsat-8 OLI and Sentinel-2A MSI data to identify the most suitable index for BA detection in this region. Then, we refined this data through the GEOBIA-based model. The results showed that the Burned Area Index (BAI) was the most suitable index for BA mapping (M index >1.5) for both sensors. Our model allowed detecting more than 80% of small BA and also presented high Dice coefficient values (~0.70) with low omission and commission errors (0.22 and 0.32, respectively). Such combined approach corresponds to a novel contribution to the BA detection in the Brazilian Amazon region and for enhancing the operational product generation.

Keywords: Fires mapping. Tropical forest. Landsat-8 OLI. Sentinel-2A MSI.

Resumo: O mapeamento refinado de áreas queimadas (AQ) na Amazônia brasileira ainda é um desafio. A principal dificuldade na detecção de AQ para grandes áreas é a presença de nuvens e corpos hídricos. A utilização de diferentes fontes de dados de imagens de sensoriamento remoto de média resolução espacial pode fornecer uma maior disponibilidade de imagens livres de nuvens, além de reduzir as incertezas associadas aos dados de resolução espacial grosseira (>250m), os quais podem subestimar ou superestimar AQ e dificultar a detecção de AQ pequenas (<0,1km²). Neste estudo, propomos uma metodologia inovadora baseada no uso de índices espectrais e análise de imagem baseada em objetos geográficos (GEOBIA), usando imagens de média resolução espacial para melhorar a detecção de AQ em áreas teste na Amazônia. Primeiramente, avaliamos o desempenho de nove índices espectrais em duas áreas de estudo obtidos a partir de cenas do Landsat-8 OLI e Sentinel-2A MSI para identificar o índice mais adequado para a detecção de AQ. Em seguida, refinamos esses dados através do modelo baseado em GEOBIA. Os resultados mostraram que o Índice de Área queimada (BAI) foi o mais adequado para o mapeamento de AQ (índice M>1,5) para ambos os sensores. Nosso modelo permitiu detectar mais de 80% das AQs pequenas (<1 km²) e também apresentou altos valores de coeficiente Dice (~0,70) com baixos erros de omissão e comissão (0,22 e 0,32, respectivamente). Essa abordagem integrada correspondeu a uma contribuição inédita para a detecção de AQs na região amazônica e para o aprimoramento da geração de produtos operacionais.

Palavras-chave: Mapeamento de áreas queimadas. Floresta tropical. Landsat-8 OLI. Sentinel-2A MSI.

1 INTRODUCTION

The Brazilian Amazon covers an area of 4.2 million km² or 49% of the Brazilian territory (IBGE, 2004), and plays an important role to the global climate regulation (VAN DER WERF et al., 2010; ARAGÃO et al., 2018). Nonetheless, forest and understory fires (ALENCAR; NEPSTAD; DIAZ, 2006; MORTON et al., 2011), deforestation-related fires (ARAGÃO; SHIMABUKURO, 2010; FANIN; VAN DER WERF, 2015) and fires for land management (LIMA et al., 2012; ANDERSON et al., 2015) are some of the human-induced typical phenomena in the Brazilian Amazon, challenging the reduction of the carbon emission as well as the preservation of the ecosystem services (ARAGÃO et al., 2014). In the Brazilian Amazon, the burning occurrence is mostly related to induced and uncontrolled fires for land management, aiming to prepare and transform the land for many economic purposes, such as agriculture and cattle ranching (FEARNSIDE, 2005; VAN DER WERF et al., 2010). Besides that, such activities, whenever associated with more intense and frequent droughts, have contributed to increase fires in the region (ARAGÃO et al., 2007; ALENCAR et al., 2015). In this context, burned areas (BA) detection is essential in order to assess its extent, to quantify impacted areas, as well as and to monitor the vegetation regeneration (KATAGIS; GITAS; MITRI, 2014; MOUILLOT et al., 2014).

BA mapping in the Brazilian Amazon is typically performed based on remote sensing (RS) methods using coarse spatial resolution (>250m) satellite data (MOUILLOT et al., 2014; SHIMABUKURO et al., 2015), because they often operate with high temporal frequency. Nonetheless, coarse spatial resolution data may underestimate or overestimate the spatial distribution of small BA (<0.1km²) (LARIS, 2005; MIETTINEN et al., 2013; SHIMABUKURO et al., 2015).

Despite presenting a longer revisiting time, medium spatial resolution satellite images, ranging from 10 to 50 meters (EHLERS et al., 2002), provides more detailed information and are more suitable to analyze the extent, distribution, spectral and biophysical characteristics of BA with higher reliability. Moreover, they have the potential to increase the availability of suitable images through data fusion (LATORRE et al., 2007; ARAI et al., 2011), for instance, involving Landsat-8 OLI (WULDER et al., 2012) and Sentinel-2A MSI (DRUSCH et al., 2012) satellite data.

A number of studies of BA mapping have achieved promising results using spectral indices (BASTARRIKA; CHUVIECO; MARTÍN, 2011; LIBONATI et al., 2012; BASTARRIKA et al., 2014; CARDOZO et al., 2014; PEREIRA et al., 2016). However, the detection of small BA (<0.1km²) is often overlooked by researches. Due to its relevance for the Brazilian Amazon and considering the lack of such studies, we developed a novel methodology to improve the BA mapping using medium spatial resolution images, spectral indices, and the approach known as geographic object-based image analysis (GEOBIA). GEOBIA usage enables: object-oriented image classification rather than pixel-per-analysis (HAY; CASTILLA, 2006; BLASCHKE, 2010); the insertion of knowledge about the region of interest in the classification model; and the extraction of both spectral and spatial features information (PINHO et al., 2012). Nevertheless, a segmentation algorithm is required in GEOBIA framework (CHUVIECO; MARTÍN; PALACIOS, 2002), which might refine the BA mapping.

The present study was guided by the following main questions: (1) Which spectral index has the greatest ability to individualize BA from other targets in the Brazilian Amazon?; (2) What are the differences in the performance of such indices in different medium resolution images?; (3) Can the BA detection method based on GEOBIA refine BA mapping? To answer such questions, we first assessed the performance of nine spectral indices aiming to identify the most suitable index for BA mapping. Then, we refined this result applying a GEOBIA-based model. Four images, two from Landsat-8 OLI and two from Sentinel-2A MSI, in two different study areas were used.

2 MATERIAL AND METHODS

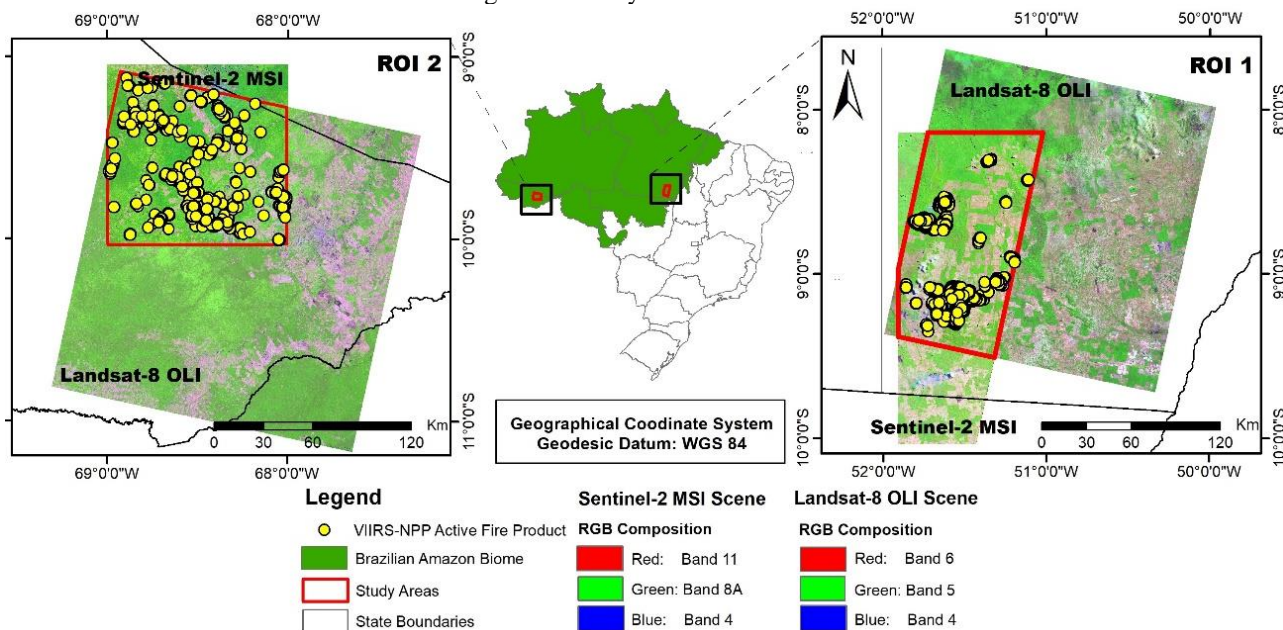
2.1 Study sites

The regions of interest (ROI) are situated in the Brazilian states of Pará (ROI 1) and Acre (ROI 2),

north and northwest of the Amazon biome, respectively (Figure 1). These areas were selected according to the occurrence of burning events identified by NOAA VIIRS-NPP (375m) active fire product, and delimited by the overlapping of Landsat-8 OLI and Sentinel-2A MSI scenes.

In our study areas, the main land-use and land-cover are composed by forest, pasture and small agriculture. According to TerraClass (ALMEIDA et al., 2016), for the year of 2014, the main land cover classes in ROI 1 were forest (68.65%) and pasture (24.98%), meanwhile, in ROI 2, it was forest (97.37%). Most of the burned area are related to pasture maintenance (ROI 1) and deforestation (ROI 2), often occurring in forest areas.

Figure 1 – Study sites localization.



Source: The authors (2020).

2.2 Data acquisition

Two cloud-free Landsat-8 OLI scenes (WRS 2 – Worldwide Reference System 2, path/row 002/67 and path/row 224/66) were obtained on August 24th, 2016 (ROI 1) and August 27th, 2016 (ROI 2) from U.S. Geological Survey (freely available at <https://www.earthexplorer.usgs.gov/>) in surface reflectance (High-Quality level) with radiometric and geometric correction in UTM/WGS84 projection and also corrected for atmospheric conditions (VERMOTE et al., 2016).

Two cloud-free Sentinel-2A MSI scenes were obtained on the same date as Landsat-8 OLI imageries, from Copernicus Scientific Data Hub (ESA – European Space Agency) (freely available at <http://www.scihub.copernicus.eu/>) as top-of-atmosphere (TOA) level-1C (L1C) product with radiometric and geometric corrections in UTM/WGS84 projection.

2.3 Reference dataset

A specialist produced the BA reference map for both ROI 1 and ROI 2 based on the method developed by Shimabukuro et al. (2009). Such method uses the shade fraction image, derived from the Linear Spectral Mixture Model (LSMM) (SHIMABUKURO; SMITH, 1991). Subsequently, the K-means unsupervised classification algorithm was applied followed by a manual post classification image edition. The post-classification edition was carried out by a skilled human interpreter using natural color composites, aiming to minimize omission and commission errors produced by the automatic classification algorithms (ALMEIDA-FILHO; SHIMABUKURO, 2002; PIROMAL et al., 2008; LIMA et al., 2012; CARDOZO et al., 2014; SHIMABUKURO et al., 2015; ANDERSON et al., 2015). The total of BA generated were: 188.69 km² (ROI 1 – Landsat-8), 174.99 km² (ROI 1 – Sentinel-2A), 89.39 km² (ROI 2 – Landsat-8) and 82.39 km² (ROI 2 –

Sentinel-2A). The dataset can be found at: <<https://doi.org/10.6084/m9.figshare.8104736>>.

2.4 Preprocessing and data compatibilization

First of all, we applied in all Sentinel-2A MSI bands an atmospheric correction performed by Sen2Cor processor (MAIN-KNORN et al., 2015; MÜLLER-WILM, 2017). A Level-2A bottom-of-atmosphere (BOA) reflectance product was created and resampled to 20m pixel size. We then co-registered Landsat-8 OLI and Sentinel-2A MSI images for both study areas (RMS = 0.21 for ROI 1 and RMS = 0.25 for ROI2) using feature-based registration method (FONSECA; MANJUNATH, 1996; YAN et al., 2016). Six corresponding bands with similar wavelength from Landsat-8 OLI and Sentinel-2A MSI were selected (Blue, Green, Red, Near Infrared (NIR), SWIR 1, and SWIR 2). In this study, Landsat-8 OLI and Sentinel-2A MSI dataset were used independently, that is, no bias correction was applied, since both sensors can be considered similar (MANDANICI; BITELLI, 2016).

2.5 Spectral indices application

We calculated four vegetation indices and five burn indices, for both study sites (Chart 1). The BAIM, CSI, and NBR burn indices were adapted as both Landsat-8 and Sentinel-2A satellites operate with two SWIR bands. The reference data were used to create the dataset of burned and unburned areas, enabling the identification of the indices with the highest performances.

Chart 1 – Selected spectral indices. Legend: ρ_B = blue reflectance band; ρ_{Red} = red reflectance band; ρ_{NIR} = near-infrared reflectance band; ρ_{SWIR} = short wavelength infrared band; ρ_{LSWIR} = long short wavelength infrared band.

Spectral Indices	Initials	Formula	Reference
Simple Ratio	SR	$\frac{\rho_{NIR}}{\rho_{Red}}$	Birth and McVey (1968)
Normalized Difference Vegetation Index	NDVI	$\frac{(\rho_{NIR} - \rho_{Red})}{(\rho_{NIR} + \rho_{Red})}$	Rouse et al. (1973)
Soil Adjusted Vegetation Index	SAVI	$\frac{(1 + 0.5)(\rho_{NIR} - \rho_{Red})}{(\rho_{NIR} + \rho_{Red} + 0.5)}$	Huete (1988)
Enhanced Vegetation Index	EVI	$\frac{2.5(\rho_{NIR} - \rho_{Red})}{(1 + \rho_{NIR} + 6.0 \rho_{Red} - 7.5 \rho_B)}$	Huete et al (2002)
Burned Area Index	BAI	$\frac{1}{(0.1 - \rho_{Red})^2 + (0.06 - \rho_{NIR})}$	Chuvieco, Martín and Palacios (2002)
Burned Area Index Modified	BAIM	$\frac{1}{(\rho_{NIR} - 0.05)^2 + (\rho_{LSWIR} - 0.2)^2}$	Martín et al. (2006)
Normalized Burn Ratio	NBR	$\frac{\rho_{NIR} - \rho_{SWIR}}{\rho_{NIR} + \rho_{SWIR}}$	Key and Benson (2006)
Mid-Infrared Burn Index	MIRBI	$10 \rho_{LSWIR} - 9.8 \rho_{SWIR} + 2$	Trigg and Flasse (2001)
Char Soil Index	CSI	$\frac{\rho_{NIR}}{\rho_{LSWIR}}$	Smith et al. (2007)

Source: The authors (2020).

2.6 Spectral indices statistical analysis and threshold test

The statistical tests were performed to verify the statistic differences of burned/unburned areas, which were assessed by Wilcoxon-Mann-Whitney test (Mann-Whitney U-test) (DEPUY; BERGER; ZHOU, 2005). The ranking of the best spectral indices was based on the M separability index (Eq. 1) (KAUFMAN; REMER, 1994; GARCÍA; CHUVIECO, 2004; LASAPONARA, 2006; PEREIRA et al., 2016).

$$M = \frac{|\mu_b - \mu_u|}{\sigma_b + \sigma_u} \tag{1}$$

where: μ_b and μ_u are the mean values for burned and unburned areas respectively, and σ_b and σ_u are the corresponding standard deviations.

The M separability index was used to measure if the mean (μ_b) and the standard deviation (σ_b) of BA were statistically significant distant from the unburned areas. M separability index larger than one ($M > 1$) indicates good separation, while values smaller than one unit ($M < 1$) reveals poor discriminatory power (KAUFMAN; REMER, 1994; LASAPONARA, 2006; PEREIRA et al., 2016).

Next, the threshold tests were performed to identify the best spectral index for detecting ‘core’ pixels within BA (CHUVIECO; MARTÍN; PALACIOS, 2002; GARCÍA; CHUVIECO, 2004). In such a way, the histogram of the best spectral index for BA detection was divided in two regions of most and least accumulated pixels values, based on its statistical parameters of average (μ) and standard deviation (σ). The region between the distances of +1.0, +1.5, +2.0 and -1.0, -1.5, -2.0 standard deviations ($\pm 1.0, 1.5, 2.0 \sigma$) in relation to the average (μ) were used as threshold tests. After that, we generated an error matrix and a precision-recall curve to support the results. The precision-recall curve is described by two metrics derived from error matrix (Eq. 2 and 3).

$$Precision = \frac{T_p}{T_p + F_p} \quad (2)$$

$$Recall = \frac{T_p}{T_p + F_N} \quad (3)$$

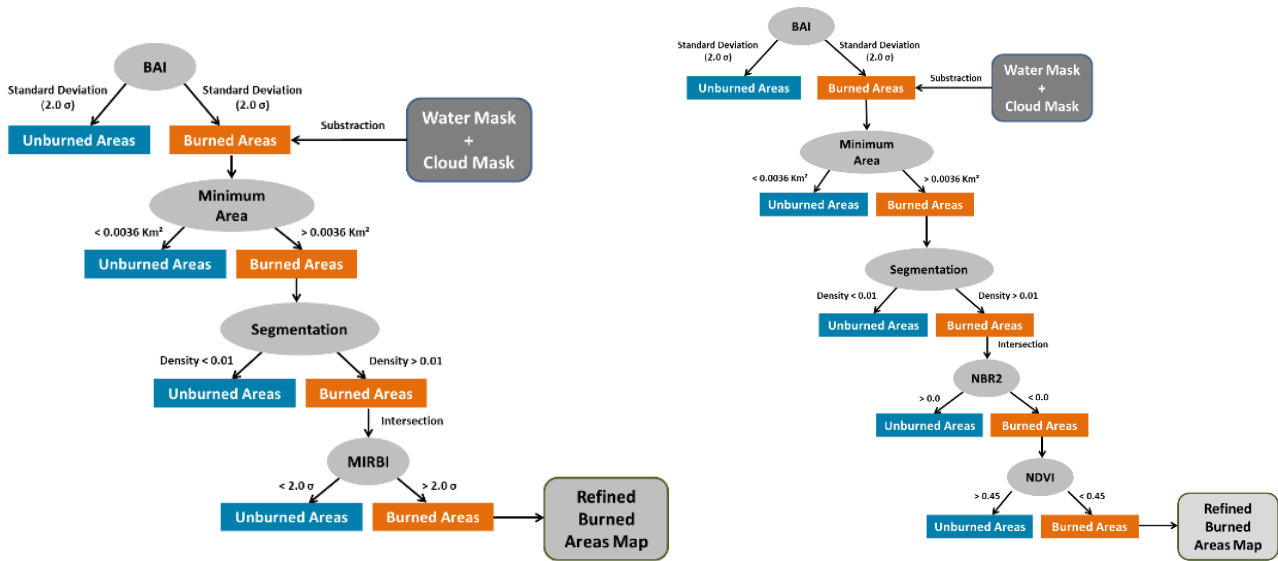
where: T_p is the number of true positives, F_p is the number of false positives and F_N is the number of false negatives in the confusion matrix.

2.7 GEOBIA-based burned areas detection model

As a final step, a GEOBIA-based model was built for each ROI in order to refine the BA detection through a rule-decision tree method (Figure 2). The BA detection was refined by delineating each burned area with a shape refinement algorithm (CHUVIECO; MARTÍN; PALACIOS, 2002; HAY; CASTILLA, 2006; BLASCHKE, 2010; BASTARRIKA; CHUVIECO; MARTÍN, 2011; PINHO et al., 2012; BASTARRIKA et al., 2014). Firstly, water and cloud masks were applied to eliminate the errors related to the misdetection of targets with similar spectral behavior of BA, such as water bodies, cloud and cloud-shadow features. The water mask was extracted from Namikawa, Körting, and Castejon (2016) and the cloud and cloud-shadow masks were generated by Fmask (Function of Mask) algorithm (ZHU; WOODCOCK, 2012; ZHU, WANG; WOODCOCK, 2015). Secondly, a minimum area threshold of approximately 0.0036 km² (or four pixels) was defined in order to avoid false positive detection. Next, a multi-resolution algorithm was used in the segmentation process (BAATZ; SCHÄPE, 2000), for both sensors and study sites, with the following thresholds: scale: 10; shape: 0.1; and compactness: 0.5. The segmentation parameters were defined based on exhaustive empirical tests in order to maintain a standard to enable its replication in future studies. Segments with BA density higher than 0.01 were filtered.

An intersection procedure was used as a second spectral index to ensure the BA in each segment. The selection of the second spectral index was based on the M separability index ranking, where the discrimination ability of BA was greater than one (M separability index > 1). We also tested empirically a plenty of thresholds before selecting the most suitable one, following the procedures of the GEOBIA’s attribute selection step. The MIRBI and NBR2 were selected for the ROI 1 and ROI 2, respectively. Finally, for ROI 2, we also selected the NDVI to eliminate false positives in forest cover because most of BA identified in this study presented post-fire charcoal signal response. Moreover, aiming to support the refined BA detection analysis, we evaluated the size of the BA, and quantified the number of fire occurrence one month before the imagery obtained (due to signal persistence of BA after burning) through the spatial agreement of NOAA VIIRS-NPP (375m) active fire products and BA mapping. The last analyze was proposed to verify if our BA-model and reference data were detecting occurred fires, indeed, or if they detected false positive targets.

Figure 2 – GEOBIA-based burned areas detection model applied in the best spectral index in order to refine the BA detection for ROI 1 (A) and ROI 2 (B).



Source: The authors (2020).

2.8 Accuracy assessment

The accuracy assessment was applied for both threshold tests and after the refined BA maps generated by GEOBIA-based model according to the methodologies proposed by Oliva and Schroeder (2015) and Padilla et al. (2015). The method consisted of spatial intersection of the reference data with the BA mapped result. We generated standard confusion matrices and calculated omission error (Oe), commission error (Ce), overall accuracy (OA), Dice coefficient (DC) and relative bias (RelB) (PADILLA et al., 2015; PADILLA et al., 2017; RAMO; CHUVIECO, 2017; MITHAL et al., 2018). The DC (DICE, 1945) combines both Oe and Ce errors in a single metric, which is useful to verify product accuracies as well as to summarize measures of accuracy of the category “burned areas” (PADILLA et al., 2015; PADILLA et al., 2017) (Eq. 4).

$$DC = \frac{2 T_P}{2(T_P + F_p + F_N)} \tag{4}$$

where: T_P is the number of true positives, F_p is the number of false positives and F_N is the number of false negatives in the confusion matrix.

The RelB (Eq. 5) is a measure of bias relative to the reference BA and express to end-users the relative BA product error balance (MOUILLOT et al., 2014; PADILLA et al., 2015; PADILLA et al., 2017).

$$RelB = \frac{F_p - F_N}{N} \tag{5}$$

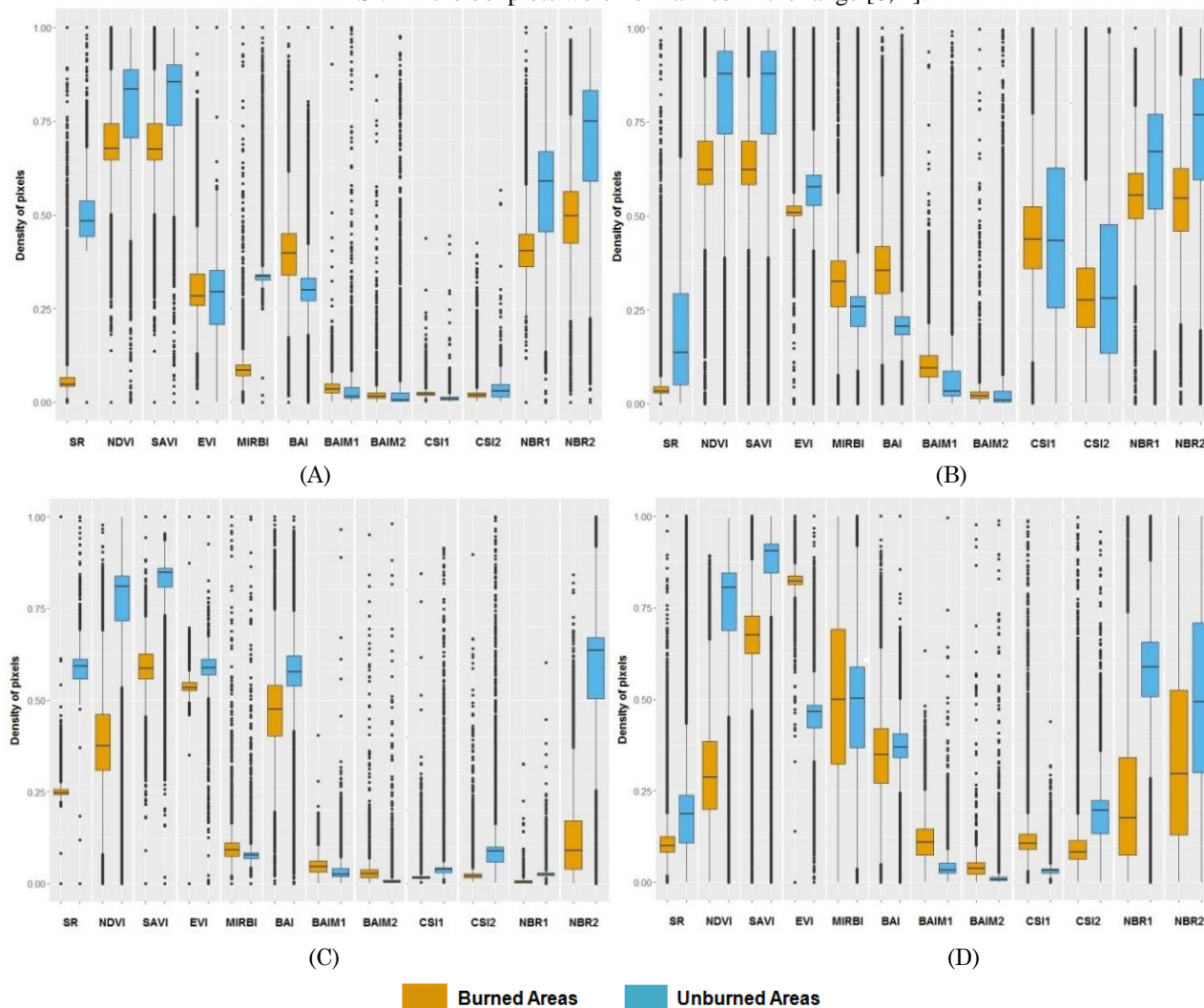
where: F_p is the number of false positives, F_N is the number of false negatives in the confusion matrix and N is the total number of elements in reference data. The RelB values indicate whether a product overestimates (positive sign) or underestimates (negative sign) the extent of BA (RAMO; CHUVIECO, 2017).

3 RESULTS

3.1 Spectral indices analysis

The results of the comparison between spectral indices BA detection and reference data for each study area are presented in boxplots (Figure 3). The histogram of each index for each ROI is available on Supplementary Material A (Available at: <https://doi.org/10.6084/m9.figshare.8104808>). For ROI 1 (Figure 3.A, 3.B), we observed that most of the spectral indices presented burned and unburned values overlapped as well as outliers that increase the misdetection for both sensors. However, for ROI 2 (Figure 3.C, 3.D) the boxplots patterns are reversed once most of the indices present good separability and they are able to discriminate these classes. Besides that, they present lower overlaps, which indicate greater ability to distinguish burned and unburned areas. Nonetheless, the number of outliers is considerable. The differences observed in the boxplots of Landsat-8 OLI and Sentinel-2A MSI in ROI 2 may be attributed to the relative spectral reflectance of vegetation types in terms of density and spatial heterogeneity characteristics. For both study areas, the Landsat-8 OLI images presented less scattering, evidencing the difficulty to determine the BA or to define an appropriate threshold.

Figure 3 – Normalized spectral indices boxplots for ROI 1: (A) Boxplots for Landsat-8 OLI; (B) Boxplots for Sentinel-2A MSI. Normalized spectral indices boxplots for ROI 2: (C) Boxplots for Landsat-8 OLI; (D) Boxplots for Sentinel-2A MSI. All the boxplots were normalized in the range [0, 1].

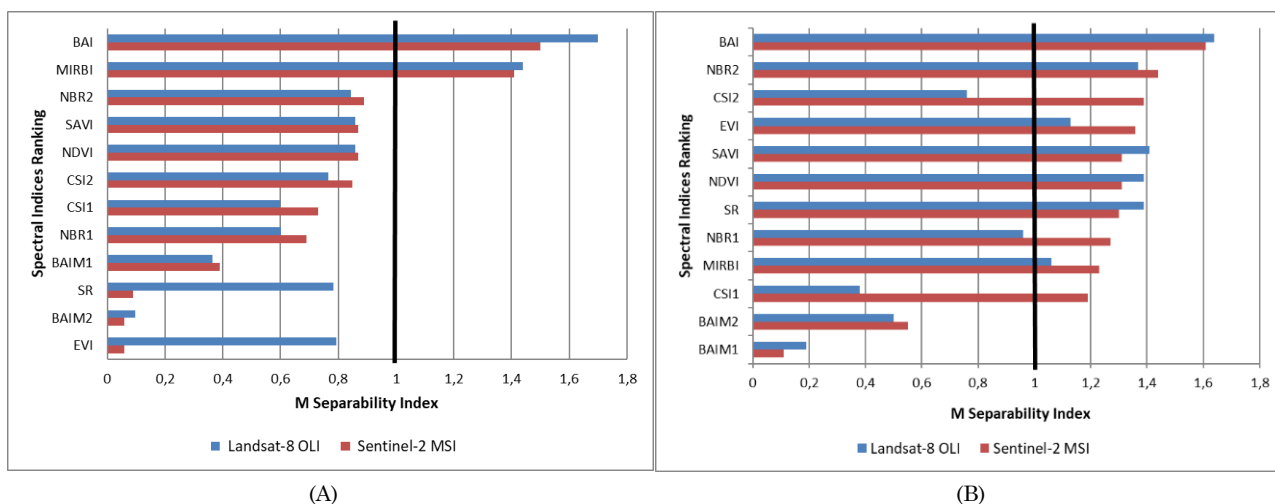


Source: The authors (2020).

3.2 Spectral indices ranking

The spectral indices ranking is presented in Figure 4. The Mann-Whitney U-test ($p < 0.05$) identified the differences between burned and unburned areas for the 12 indices tested ($p = 2.2e-16$). It was observed for ROI 1 that only BAI and MIRBI indices presented a significant separation ($M > 1$) for both sensors, while the other indices were considered poor ($M < 1$). For the ROI 2, seven indices from Landsat-8 OLI and ten indices from Sentinel-2A MSI were considered appropriate ($M > 1$). The large M values differ between ROI 1 and ROI 2, which can be explained by the presence of different land covers and low-reflectance targets in the images. For ROI 1, the presence of pasture and bare soil areas, which present low spectral signals, possibly affected the majority of the indices, generating misdetection. On the other hand, in ROI 2, the main land cover is forest, which explains the better separability and low misdetection.

Figure 4 – Spectral index ranking for ROI 1(A) and ROI 2 (B).

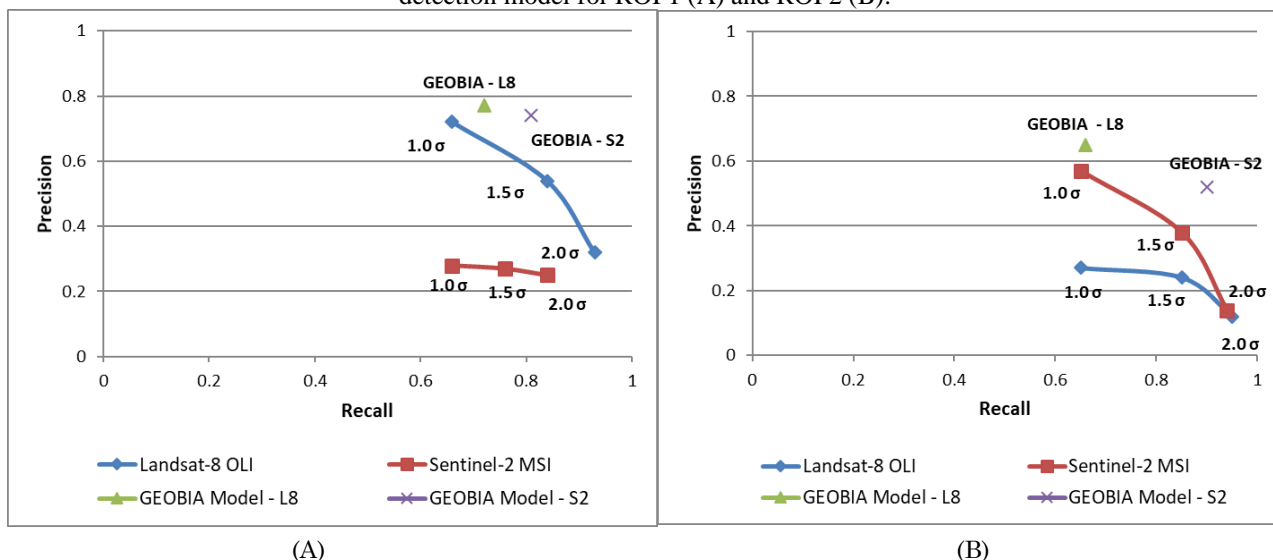


Source: The authors (2020).

3.3 Threshold tests results

The threshold tests were applied only for BAI (M separability index > 1.5) since it presented the best statistical results (Figure 4). Regarding only the best threshold for each study area and sensor, we selected the two standard deviations ($\pm 2.0 \sigma$) around the mean as the threshold to better represent the indexes variation inside the burned areas. Besides, this threshold is the most suitable that comprehended most of the BA sizes, including small BA ($< 1\text{km}^2$) (Figure 5). This value was selected since it presented the best relation between information and false positive error. The precision-recall curves for ROI 1 and ROI 2 (Figure 5) show the relation between the increasing of threshold value and the commission error ($1 - \text{precision}$) and omission error ($1 - \text{recall}$). The error matrix of this step is available in Supplementary Material B (available online at: <https://doi.org/10.6084/m9.figshare.8104808>). Although Figures 5A and 5B show high values to recall and low values to precision for the two standard deviations, we considered such threshold because it included most of the BA, especially the small BA ($< 1\text{km}^2$), and it did not omit a relevant amount of information (low omission errors). Despite the low precision value, we assumed that it would be more suitable to refine the BA detection by a GEOBIA model, minimizing the commission errors and, consequently, increasing the precision afterwards.

Figure 5 – Precision-recall curves of the tested thresholds (+/- 1,0 σ ; +/- 1,5 σ ; +/- 2,0 σ) and GEOBIA-based BA detection model for ROI 1 (A) and ROI 2 (B).



Source: The Authors (2020).

3.4 GEOBIA-based burned areas detection results and accuracy assessment

We observed the commission error reduction of approximately 51% in relation to the mean of best BAI threshold, and a DC increase of about 58% (Table 1). There was also a gain of overall accuracy (all refined BA map ~99%). However, there was an increase of about 11% in omission error in relation to the mean of best BAI threshold. Besides, RelB also presented a significantly decrease of about 85% considering the RelB mean of best BAI threshold. The refined BA maps and the accuracy assessment results for the GEOBIA-based BA mapping are presented in Supplementary Material C and D, respectively (Available online at: <https://doi.org/10.6084/m9.figshare.8104808>).

Table 1 – Commission error (Ce), omission error (Oe), Dice coefficient (DC) and relative bias (RelB) for refined BA map.

	ROI 1		ROI 2		Mean
	Landsat-8 OLI	Sentinel-2A MSI	Landsat-8 OLI	Sentinel-2A MSI	
Oe	0.28	0.18	0.34	0.10	0.22
Ce	0.22	0.26	0.34	0.47	0.32
DC	0.75	0.78	0.66	0.67	0.71
RelB	38.82	49.82	30.66	65.90	46.3

Source: The authors (2020).

The GEOBIA-based BA mapping analysis was evaluated by the size of BA mapped (Table 2), as well as the number of fire occurrence one month before the imagery acquisition (Table 3). The size of most of the reference polygons was lower than 0.1 km², values between 82% and 89% (Table 2). For both ROIs, the percentage of total number of BA mapped was considered very similar to the reference, while ROI 1 presents about 3% of large BA (> 0.1 km²), in ROI 2 less of 0.7% of large BA were identified. In such a way, regarding the small sizes, the proposed methodology was suitable. However, some of the large BA were not detected. That could be explained by the segmentation method configuration adopted, which prioritizes small objects. In addition, if we consider the total area mapped by refined BA model, we observe in ROI 1 a BA underestimation in the order of 7% for Landsat-8 OLI image and an overestimation of around 10% for Sentinel-2A MSI image. For ROI 2, a burned area overestimation was observed in both sensors data of the order of 2% for Landsat-8 OLI image and about of 64% for Sentinel-2A MSI image.

Table 2 – Frequency distribution of burned areas in both study areas and sensors. Four intervals (from small burned areas to large burned areas) were defined. L8 = Landsat-8 and S2A = Sentinel-2A.

Reference Polygon Burned Area Size (a) [km ²]	Percentage of Total Number of Burned Areas (Reference ROI 1)		Percentage of Total Number of Burned Areas Detected ROI 1		Percentage of Total Number of Burned Areas (Reference ROI 2)		Percentage of Total Number of Burned Areas Detected ROI 2	
	[%]		[%]		[%]		[%]	
	L8 OLI	S2A MSI	L8 OLI	S2A MSI	L8 OLI	S2A MSI	L8 OLI	S2A MSI
a < 0.1	85.40	82.10	84.45	82.27	86.95	87.93	89.35	89.77
0.1 < a < 0.3	7.25	8.90	7.63	9.15	9.62	8.89	9.44	8.98
0.3 < a < 0.9	4.30	5.35	4.60	5.05	2.72	2.51	1.11	1.25
a > 0.9	3.05	3.65	3.33	3.53	0.71	0.77	0.10	-

Source: The authors (2020).

Table 3 – NOAA VIIRS-NPP (375m) active fire product for 1 month before imagery acquisition.

Study Areas	Active fire product (Reference data)	Active fire product (Refined map)
	[observed / total occurrence]	[observed / total occurrence]
RO I 1	Landsat-8 OLI	907 / 1158 (78.32%)
	Sentinel-2A MSI	893 / 1158 (77.12%)
RO I 2	Landsat-8 OLI	556 / 620 (89.68%)
	Sentinel-2A MSI	590 / 620 (95.16%)

Source: The authors (2020).

4 DISCUSSION

For BA detection, its comprehensive BA spectral behavior is required. According to Pereira and Setzer (1993), BA in Landsat-5 TM images in the Brazilian Amazon region, are characterized by a reflectance decrease in the visible and NIR bands, and an increase in the SWIR bands. Such bands were also considered the most relevant channels in our study for BA detection, as reported by other authors (PEREIRA, 1999; BASTARRIKA; CHUVIECO; MARTÍN, 2011; LIBONATI et al., 2012; PEREIRA et al., 2016; HUANG et al., 2016; MALLINIS et al., 2017).

Efforts for BA mapping using Landsat-8 OLI and Sentinel-2A MSI imageries include the study conducted by Mallinis et al. (2017), who evaluated several spectral indices in those sensors for discriminating fire severity in a Mediterranean region. The results confirmed that NIR and SWIR bands of both sensors are more efficient for distinguishing burned from unburned areas. Huang et al. (2016) also assessed spectral indices in Sentinel-2A images for BA mapping in a bi-temporal approach and indicated such bands as the most suitable for BA studies in five different regions worldwide.

Vedovato et al. (2015) compared NBR and LSMM in a Brazilian Amazon region and reported that NBR was consistently able to distinguish BA in most cases. Nevertheless, some misdetections with bare soil and water bodies were observed due to the similar spectral responses. These authors also observed that the size of the BA affects the detection. The more fragmented and the smaller the BA, the more border errors appears.

According to the boxplots analysis and the M separability index ranking (Figure 4), BAI was considered the most suitable spectral index in both sensors and study areas. This result was probably obtained considering that BAI was designed to emphasize charcoal in post-fire images, which may present potential confusion with low-reflectance targets, such as water bodies and cloud shadows (CHUVIECO; MARTÍN; PALACIOS, 2002). Besides BAI, MIRBI also presented good performance in both ROIs and sensors (M separability index > 1) because of the single-temporal approach, which favors spectral indices that are more sensitive to recent BA. On the other hand, BAIM and CSI presented the lowest discrimination capacity, as observed by Melchiori et al. (2015). Differences of spectral indices performance for BA discrimination may occur due to several factors, such as the period between data acquisition and occurrence of fires, and the specific biophysical characteristics of the study areas, interfering in the burned spectral properties (PEREIRA, 1999). Another possibility is due to the heterogeneity of the unburned areas, which is reported in literature as a category that includes clouds and cloud shadows and numerous land covers, producing potential confusions with BA, such as borders of lakes, topographic shadows and mixed urban-vegetated areas (CHUVIECO;

CONGALTON, 1988; BASTARRIKA; CHUVIECO; MARTÍN, 2011).

Regarding the use of medium spatial resolution images, both Landsat-8 and Sentinel-2A datasets reached similar accuracies in most of the experiments. Presenting higher M separability values, the spectral indices derived from Sentinel-2A MSI images were more suitable for BA detection in ROI 2 (Figure 4), once they mostly presented higher M separability index values. The same tendency was not observed in ROI 1, remaining non-conclusive. Although the results indicate the differences of BA detection, they may be explained by factors such as: the inherent characteristics of the OLI and MSI sensors, residual effects of spatial heterogeneity generated by the resampling procedure, residual co-registration errors, acquisition methods of the sensors and by techniques used for geometric and atmospheric correction (MANDANICI; BITELLI, 2016). In some applications, this task may be overcome by the GEOBIA approach, as recommended by Novelli et al. (2016).

The selection of a fixed thresholds for BA detection might be under or overestimating such detections, once potential confusion targets are included, such as: the clouds, borders of lakes, bare soils, and topographic shadows (PEREIRA, 1999; BASTARRIKA; CHUVIECO; MARTÍN, 2011). For burned land mapping, Chuvieco, Martín and Palacios (2002) emphasized that the thresholds selection for BAI should be very strict, since this index shows a high variability within charcoal areas. In this sense, the GEOBIA-based BA detection model, as suggested by Chuvieco, Martín and Palacios (2002), was applied to minimize the omission and commission errors. Such errors were low in the proposed methodology, about 0.22 and 0.32, respectively. In addition, Table 2 and Table 3 showed that the proposed methodology allowed the inclusion of small BA (more than 80%) and presented high agreement with the reference map. Therefore, it represents an improvement for the Brazilian Amazon region mapping that might be well performed by medium spatial resolution data, as reported by Anderson et al. (2015) and Shimabukuro et al. (2015). Besides, we noted a substantial decrease of the burned area overestimation in relation to the best BAI fixed threshold mapping, which still can be improved by reviewing the fixed segmentation configuration adopted or testing other filtering elements.

5 CONCLUSIONS

We developed a methodology based on spectral indices and GEOBIA to refine the BA detection in two regions of the Brazilian Amazon, using Landsat-8 OLI and Sentinel-2A MSI sensors. This study indicated that BAI ($M \text{ index} > 1.5$) was the best spectral index for BA mapping in our study sites and for both Landsat-8 OLI and Sentinel-2A MSI sensors, considering a single-temporal date approach. These indices were not previously studied for BA mapping, especially in medium spatial resolution images, which represents a novelty itself. However, different indices, such as MIRBI and NBR2 also presented elevated M index values and good distinguishing ability between burned and unburned areas in our sites, demonstrating that NIR and SWIR spectral regions are crucial for BA detection. In contrast, BAIM and CSI presented poor results and therefore lower separability. In such a way, they are less indicated for the Brazilian Amazon region studies.

This work also demonstrated that for refined BA mapping only the threshold method is not sufficient, once it detects burned 'core' areas, but presents higher omission and commission errors. A second phase, which included a refined BA detection model based on GEOBIA, allowed a better delineation of burned areas and a decrease in the misdetection. Nonetheless, the proposed methodology applied in medium spatial resolution imagery presents a better balancing of omission and commission errors (mean of 0.22 and 0.32, respectively) for BA mapping, as well as a high DC (about 0.70) and a low RelB (about 46.3). Moreover, our methodology allowed including small BA (more than 80%) which is an improvement for the Brazilian Amazon region mapping and BA overall estimation. Such approach is a novel contribution to the BA detection in the Brazilian Amazon and can be enhanced for an operational product generation. However, the fixed segmentation configuration and thresholds definition in the GEOBIA may not be suitable for the whole Amazon region.

For further researches, the methodology should be tested in other study areas (due to Amazon's heterogeneity) and medium resolution images, such as CBERS-4 MUX and Resourcesat-2 LISS. In this manner, these studies would contribute to increase the data coverage and availability for the Brazilian Amazon and to support the generation of refined BA products.

Acknowledgement

The authors thank the financial support from Brazil's Coordination for the Improvement of Higher Education Personnel (CAPES), the Brazil's National Council for Scientific and Technological Development (CNPq), processes 309247/2016-0, 442650/2018 and 140377/2018-2, the São Paulo Research Foundation (FAPESP, Process 2016/02018-2) and Inter-American Institute for Global Change Research (IAI), process: SGP-HW 016.

Conflicts of interest

The authors declare no conflict of interest.

Authors contributions

Thales Penha, Thales Körting, Leila Fonseca, Celso Silva Junior, Mikhaela Pletsch, Liana Anderson and Fabiano Morelli conceptualized and designed the research. Thales Penha performed the data processing, spectral indices application, statistical analysis and accuracy assessment, as well as he wrote the paper. Celso Silva Junior and Mikhaela Pletsch supported in the methodology execution and referenced data processing. Thales Körting, Leila Fonseca, Liana Anderson and Fabiano Morelli contributed with insights about analysis and methods. All authors equally contributed with the manuscript writing.

References

- ALENCAR, A.; NEPSTAD, D.; DIAZ, M. C. V. Forest understory fire in the Brazilian Amazon in ENSO and non-ENSO years: area burned and committed carbon emissions. **Earth Interactions**, v. 10, n. 6, p. 1-17, 2006. DOI: 10.1175/EI150.1.
- ALENCAR, A. A.; BRANDO, P. M.; ASNER, G. P.; PUTZ, F. E. Landscape fragmentation, severe drought and the New Amazon forest fire regime. **Ecological Society of America**, vol. 25, n. 6, p. 1493–1505, 2015. DOI: 10.1890/14-1528.1.
- ALMEIDA, C. A.; COUTINHO, A. C.; ESQUERDO, J. C. D. M.; ADAMI, M.; VENTURIERI, A.; DINIZ, C. G.; DESSAY, N.; DURIEUX, L.; GOMES, A. R. High spatial resolution land use and land cover mapping of the Brazilian Legal Amazon in 2008 using Landsat-5/TM and MODIS data. **Acta Amazonica**, vol. 46, p. 291–302, 2016. DOI: 10.1590/1809-4392201505504.
- ALMEIDA-FILHO, R.; SHIMABUKURO, Y. E. Digital processing of a Landsat-TM time series for mapping and monitoring degraded areas caused by independent gold miners, Roraima State, Brazilian Amazon. **Remote Sensing of Environment**, vol. 79, n. 1, p. 42–50, 2002. DOI: 10.1016/S0034-4257(01)00237-1.
- ANDERSON, L. O.; ARAGÃO, L. E. O. C.; GLOOR, M.; ARAI, E.; ADAMI, M.; SAATCHI, S. S.; MALHI, Y.; SHIMABUKURO, Y. E.; BARLOW, J.; BERENGUER, E.; DUARTE, V. Disentangling the contribution of multiple land covers to fire-mediated carbon emissions in Amazonia during the 2010 drought. **Global Biogeochemical Cycles**, vol. 29, n. 10, p. 1739–1753, 2015. DOI: 10.1002/2014GB005008.
- ARAGÃO, L. E. O. C.; ANDERSON, L. O.; FONSECA, M. G.; ROSAN, T. M.; VEDOVATO, L. B.; WAGNER, F. H.; SILVA, C. V. J.; SILVA JUNIOR, C. H. L.; ARAI, E.; AGUIAR, A. P.; BARLOW, J.; BERENGUER, E.; MERRITT, D. N.; DOMINGUES, L. G.; GATTI, L.; GLOOR, M.; MALHI, Y.; MARENGO, J. A.; MILLER, J. B.; PHILLIPS, O. L.; SAATCHI, S. 21st Century drought-related fires counteract the decline of Amazon deforestation carbon emissions. **Nature Communications**, vol. 9, n. 536, p. 1–12, 2018. DOI: 10.1038/s41467-017-02771-y.
- ARAGÃO, L. E. O. C.; MALHI, Y.; ROMAN-CUESTA, R. M.; SAATCHI, S.; ANDERSON, L. O.; SHIMABUKURO, Y. E. Spatial patterns and fire response of recent Amazonian droughts. **Geophysical**

- Research Letters**, vol. 34, n. 7, p. 1–5, 2007. DOI: 10.1029/2006GL028946.
- ARAGÃO, L. E. O. C.; POULTER, B.; BARLOW, J. B.; ANDERSON, L. O.; MALHI, Y.; SAATCHI, S.; PHILLIPS, O. L.; GLOOR, E. Environmental change and the carbon balance of Amazonian forests. **Biological Reviews**, vol. 89, n. 4, p. 913–931, 2014. DOI: 10.1111/brv.12088.
- ARAGÃO, L. E. O. C.; SHIMABUKURO, Y. E. The incidence of fire in Amazonian forests with implications for REDD. **Science**, vol. 328, n. 5983, p. 1275–1278, 2010. DOI: 10.1126/science.1186925.
- ARAI, E.; SHIMABUKURO, Y. E.; PEREIRA, G.; VIJAYKUMAR, N. L. A multi-resolution multi-temporal technique for detecting and mapping deforestation in the Brazilian Amazon rainforest. **Remote Sensing**, vol. 3, n. 9, p. 1943–1956, 2011. DOI: 10.3390/rs3091943.
- BAATZ, M.; SCHÄPE, A. Multiresolution Segmentation: an optimization approach for high quality multi-scale image segmentation. **Journal of Photogrammetry and Remote Sensing**, vol. 58, n.3-4, p. 12–23, 2000.
- BASTARRIKA, A.; ALVARADO, M.; ARTANO, K.; MARTINEZ, M. P.; MESANZA, A.; TORRE, L.; RAMO, R.; CHUVIECO, E. BAMS: A tool for supervised burned area mapping using Landsat data. **Remote Sensing**, vol. 6, n.12, p.12360–12380, 2014. DOI: 10.3390/rs61212360.
- BASTARRIKA, A.; CHUVIECO, E.; MARTÍN, M. P. Mapping burned areas from Landsat TM/ETM+ data with a two-phase algorithm: Balancing omission and commission errors. **Remote Sensing of Environment**, vol. 115, n. 4, 2011. pp. 1003–1012. DOI: 10.1016/j.rse.2010.12.005
- BIRTH, G. S.; McVEY, G. R. Measuring the color of growing turf with a reflectance spectrophotometer. **Agronomy Journal**, vol. 60, n. 6, p. 640–643, 1968. DOI: 10.2134/agronj1968.00021962006000060016x.
- BLASCHKE, T. Object based image analysis for remote sensing. **ISPRS Journal of Photogrammetry and Remote Sensing**, vol. 65, n. 1, p. 2–16, 2010. DOI: 10.1016/j.isprsjprs.2009.06.004.
- CHUVIECO, E.; CONGALTON, R. G. Mapping and inventory of forest fires from digital processing of TM data. **Geocarto International**, vol. 3, n.4, p. 41–53, 1988. DOI: 10.1080/10106048809354180.
- CHUVIECO, E.; MARTÍN, M. P.; PALACIOS, A. Assessment of different spectral indices in the red–near-infrared spectral domain for burned land discrimination. **International Journal Remote Sensing**, vol. 23, n. 23, p. 5103–5110, 2002. DOI: 10.1080/01431160210153129.
- CARDOZO, F. S.; PEREIRA, G.; SHIMABUKURO, Y. E.; MORAES, E. C. Analysis and assessment of the spatial and temporal distribution of burned areas in the amazon forest. **Remote Sensing**, vol. 6, n. 9, p. 8002–8025, 2014. DOI: 10.3390/rs6098002.
- DEPUY, V.; BERGER, V. W.; ZHOU, Y. Wilcoxon – Mann – Whitney. In: EVERITT, BRIAN. S.; HOWELL, DAVID. C.; (Orgs.). **Encyclopedia of Statistics in Behavioral Science**. Chinchester: John Wiley & Sons, Ltd, vol. 4, 2005, 1945. p. 2118–2121.
- DICE, L. R. Measures of the amount of ecologic association between species. **Ecology**, vol. 26, n. 3, p. 297–302, 1945. DOI: 10.2307/1932409.
- DRUSCH, M.; DEL BELLO, U.; CARLIER, S.; COLIN, O.; FERNANDEZ, V.; GASCON, F.; HOERSCH, B.; ISOLA, C.; LABERINTI, P.; MARTIMORT, P.; MEYGRET, A.; SPOTO, F.; SY, O.; MARCHESE, F.; BARGELLINI, P. Sentinel-2: ESA’s optical high-resolution mission for GMES operational services. **Remote Sensing of Environment**, vol. 120, p. 25–36, 2012. DOI: 10.1016/j.rse.2011.11.026.
- EHLERS, M.; JANOWSKY, R.; GAEHLER, M. New remote sensing concepts for environmental monitoring. **Remote Sensing for Environmental Monitoring**, vol. 4545, p. 1–12, 2002. DOI: 10.1117/12.453657.
- FANIN, T.; VAN DER WERF, G. R. Relationships between burned area, forest cover loss, and land cover change in the Brazilian Amazon based on satellite data. **Biogeosciences**, vol. 12, n. 20, p. 6033–6043, 2015. DOI: 10.5194/bg-12-6033-2015.
- FEARNSIDE, P. M. Deforestation in Brazilian Amazonia: History, rates, and consequences. **Conservation Biology**, vol. 19, n. 3, p. 680–688, 2005. DOI: 10.1111/j.1523-1739.2005.00697.x.
- FONSECA, L. M. G.; MANJUNATH, B. S. Registration techniques for multisensor remotely sensed imagery.

Photogrammetric Engineering & Remote Sensing, vol. 62, p. 1049–1056, 1996.

- GARCÍA, M.; CHUVIECO, E. Assessment of the potential of SAC-C/MMRS imagery for mapping burned areas in Spain. **Remote Sensing of Environment**, vol. 92, n.3, p. 414–423, 2004. DOI: 10.1016/j.rse.2004.04.011.
- HAY, G. J.; CASTILLA, G. Object-based image analysis: Strengths, weaknesses, opportunities and threats (SWOT). **International Archives of Photogrammetry Remote Sensing and Spatial Information Sciences**, vol. 36, p. 1-3, 2006.
- HUANG, H.; ROY, DAVID P.; BOSCHETTI, L.; ZHANG, H. K.; YAN, L.; KUMAR, S. S.; GOMEZ-DANS, J.; LI, J. Separability analysis of Sentinel-2A Multi-Spectral Instrument (MSI) data for burned area discrimination. **Remote Sensing**, vol. 8, n. 10, p. 873-891, 2016.. DOI: 10.3390/rs8100873.
- HUETE, A.; DIDAN, K; MIURA, T.; RODRIGUEZ, E. P.; GAO, X.; FERREIRA, L. G. Overview of the radiometric and biophysical performance of the MODIS vegetation indices. **Remote Sensing of Environment**, vol. 83, p. 195–213, 2002. DOI: 10.1016/S0034-4257(02)00096-2.
- HUETE, A. R. A soil-adjusted vegetation index (SAVI). **Remote Sensing of Environment**, vol. 25, p.295–309, 1988. DOI: 10.1016/0034-4257(88)90106-X.
- INSTITUTO BRASILEIRO DE ESTATÍSTICA E GEOGRAFIA (IBGE). Mapa de Biomassas do Brasil, primeira aproximação. Rio de Janeiro: IBGE, 2004. Available online: <https://ww2.ibge.gov.br/home/presidencia/noticias/21052004biomashtml.shtm> (accessed on 22 October 2017).
- KATAGIS, T.; GITAS, I.; MITRI, G. An object-based approach for fire history reconstruction by using three generations of Landsat sensors. **Remote Sensing**, v. 6, n. 6, p. 5480–5496, 2014. DOI: 10.1071/WF12055.
- KAUFMAN, Y. J.; REMER, L. A. Detection of forests using mid-IR reflectance: An application for aerosol studies. **IEEE Transactions on Geoscience and Remote Sensing**, vol. 32, n. 3, p. 672–683, 1994. DOI: 10.1109/36.297984.
- KEY, C. H.; BENSON, N. C. Landscape assessment: Sampling and analysis methods. **USDA Forest Service General Technical Report RMRS-GTR-164-CD**, pp. 1–55, 2006.
- LARIS, P. S. Spatiotemporal problems with detecting and mapping mosaic fire regimes with coarse-resolution satellite data in savanna environments. **Remote Sensing of Environment**, vol. 99, p. 412–424, 2005. DOI: 10.1016/j.rse.2005.09.012.
- LASAPONARA, R. Estimating spectral separability of satellite derived parameters for burned areas mapping in the Calabria region by using SPOT-Vegetation data. **Ecological Modelling**, vol. 196, n. 1–2, p. 265–270, 2006. DOI: 10.1016/j.ecolmodel.2006.02.025.
- LATORRE, M. L.; CARVALHO JUNIOR, O. A.; SANTOS, J. R.; SHIMABUKURO, Y. E. Integração de dados de sensoriamento remoto multi-resoluções para a representação da cobertura da terra utilizando campos contínuos de vegetação e classificação por árvores de decisão. **Revista Brasileira de Geofísica**, vol. 25, n. 1, p. 63–74, 2007.
- LIBONATI, R.; DACAMARA, C. C.; PEREIRA, J. M. C; PERES, L. F. Retrieving middle-infrared reflectance using physical and empirical approaches: Implications for burned area monitoring. **IEEE Transactions on Geoscience and Remote Sensing**, vol. 50, n. 1, p. 281–294, 2012. DOI: 10.1109/TGRS.2011.2160186.
- LIMA, A.; SILVA, T. S. F.; ARAGÃO, L. E. O. C. FEITAS, R. M.; ADAMI, M.; FORMAGGIO, A. R.; SHIMABUKURO, Y. E. Land use and land cover changes determine the spatial relationship between fire and deforestation in the Brazilian Amazon. **Applied Geography**, vol. 34, p. 239–246, 2012. DOI: 10.1016/j.apgeog.2011.10.013.
- MAIN-KNORN, M.; PFLUG, B.; DEBAECKER, V.; LOUIS, J. Calibration and validation plan for the I2A processor and products of the Sentinel-2 mission. **International Archives of the Photogrammetry, Remote Sensing and Spatial Information Sciences - ISPRS Archives**, vol. 40, n. 73, p. 1249–1255,

2015. DOI: 10.5194/isprsarchives-XL-7-W3-1249-2015.

- MALLINIS, G.; MITSOPOULOS, I.; CHRYSAFI, I. Evaluating and comparing Sentinel 2A and Landsat-8 Operational Land Imager (OLI) spectral indices for estimating fire severity in a Mediterranean Pine ecosystem of Greece. **GIScience and Remote Sensing**, vol. 55, n. 1, p. 1-18, 2017. DOI: 10.1080/15481603.2017.1354803
- MANDANICI, E.; BITELLI, G. Preliminary comparison of Sentinel-2 and Landsat 8 imagery for a combined use. **Remote Sensing**, vol. 8, n. 12, p. 1014-1024, 2016. DOI: 10.3390/rs8121014.
- MARTÍN, M. P.; GÓMEZ, I.; CHUVIECO, E. Burnt Area Index (BAIM) for burned area discrimination at regional scale using MODIS data. **Forest Ecology and Management**, vol. 234, p. S221, 2006. DOI: 10.1016/j.foreco.2006.08.248.
- MELCHIORI, A. E.; CÂNDIDO, P. A.; LIBONATI, R.; MORELLI, F.; SETZER, A. W.; DE JESUS, S. C.; FONSECA, L. M. G.; KÖRTING, T. S. Spectral indices and multi-temporal change image detection algorithms for burned area extraction in the Brazilian Cerrado. In: SIMPÓSIO BRASILEIRO DE SENSORIAMENTO REMOTO - SBSR, 17, 2015, João Pessoa. **Anais...** João Pessoa: INPE, 2015, p.643-650.
- MIETTINEN, J.; HYER, E.; CHIA, A. S.; KWOH, L. K.; LIEW, S. C. Detection of vegetation fires and burnt areas by remote sensing in insular Southeast Asian conditions: current status of knowledge and future challenges. **International Journal of Remote Sensing**, vol. 34, n. 12, p. 4344-4366, 2013. DOI: 10.1080/01431161.2013.777489.
- MITHAL, V.; NAYAK, G.; KHANDELWAL, A.; KUMAR, V.; NEMANI, R.; OZA, N. Mapping burned areas in tropical forests using a novel machine learning framework. **Remote Sensing**, vol. 10, n. 1, p. 69, 2018. DOI: 10.3390/rs10010069.
- MORTON, D. C.; DEFRIES, R. S.; NAGOL, J.; SOUZA, C. M.; KASISCHKE, E. S.; HURTT, G. C. DUBAYAH, R. Mapping canopy damage from understory fires in Amazon forests using annual time series of Landsat and MODIS data. **Remote Sensing of Environment**, vol. 115, n. 7, p. 1706-1720, 2011. DOI: 10.1016/j.rse.2011.03.002.
- MOUILLOT, F.; SCHULTZ, M. G.; YUE, C.; CADULE, P.; TANSEY, K.; CIAIS, P.; CHUVIECO, E. Ten years of global burned area products from spaceborne remote sensing - A review: analysis of user needs and recommendations for future developments. **International Journal of Applied Earth Observation and Geoinformation**, vol. 26, n. 1, p. 64-79, 2014. DOI: 10.1016/j.jag.2013.05.014.
- MÜLLER-WILM, U. Sentinel-2 MSI – Level-2A Prototype Processor Installation and User Manual. **European Space Agency, (Special Publication) ESA SP**, v. 49, n. 2.2, p. 1-51. 2017. Available online: <http://step.esa.int/thirdparties/sen2cor/2.2.1/S2PAD-VEGA-SUM-0001-2.2.pdf> (accessed on 22 October 2017).
- NAMIKAWA, L. M.; KÖRTING, T. S.; CASTEJON, E. F. Water body extraction from RapidEye images: an automated methodology based on hue component of color transformation from RGB to HSV model. **Revista Brasileira de Cartografia**, vol. 68, p. 1097-1111, 2016.
- NOVELLI, A.; AGUILAR, M. A.; NEMMAOUI, A.; AGUILAR, F. J.; TARANTINO, E. Performance evaluation of object based greenhouse detection from Sentinel-2 MSI and Landsat 8 OLI data: A case study from Almería (Spain). **International Journal of Applied Earth Observation and Geoinformation**, vol. 52, p. 403-411, 2016. DOI: 10.1016/j.jag.2016.07.011.
- OLIVA, P.; SCHROEDER, W. Assessment of VIIRS 375m active fire detection product for direct burned area mapping. **Remote Sensing of Environment**, vol. 160, p. 144-155, 2015. DOI: 10.1016/j.rse.2015.01.010.
- PADILLA, M.; OLOFSSON, P.; STEHMAN, S. V.; TANSEY, K.; CHUVIECO, E. Stratification and sample allocation for reference burned area data. **Remote Sensing of Environment**, vol. 203, p. 240-255, 2017. DOI: 10.1016/j.rse.2017.06.041.
- PADILLA, M.; STEHMAN, S. V.; RAMO, R.; CORTI, D.; HANTSON, S.; OLIVA, P.; ALONSO-CANAS, I.; BRADLEY, A. V.; TANSEY, K.; MOTA, B.; PEREIRA, J. M.; CHUVIECO, E. Comparing the

- accuracies of remote sensing global burned area products using stratified random sampling and estimation. **Remote Sensing of Environment**, vol. 160, p. 114–121, 2015. DOI: 10.1016/j.rse.2015.01.005.
- PEREIRA, A. A.; TEIXEIRA, F. R.; LIBONATI, R.; MELCHIORI, E. A.; CARVALHO, L. M. T. Evaluation of Spectral Indices for Burned Area Identification in Cerrado using Landsat TM Data. **Revista Brasileira de Cartografia**, vol. 68, n. 8, p. 1665–1680, 2016.
- PEREIRA, J. M. C. A comparative evaluation of NOAA/AVHRR vegetation indexes for burned surface detection and mapping. **IEEE Transactions on Geoscience and Remote Sensing**, vol. 37, n. 1, p. 217–226, 1999. DOI: 10.1109/36.739156.
- PEREIRA, M. C.; SETZER, A. W. Spectral characteristics of fire scars in Landsat-5 TM images of Amazonia. **International Journal of Remote Sensing**, vol. 14, n. 11, p. 2061–2078, 1993. DOI: 10.1080/01431169308954022.
- PINHO, C. M. D.; FONSECA, L. M. G.; KORTING, T. S.; ALMEIDA, C. M.; KUX, H. J. H. Land-cover classification of an intra-urban environment using high-resolution images and object-based image analysis. **International Journal of Remote Sensing**, vol. 33, p. 5973–5995, 2012. DOI: 10.1080/01431161.2012.675451.
- PIROMAL, R. A. S.; RIVERA-LOMBARDI, R. J.; SHIMABUKURO, Y. E.; FORMAGGIO, A. R. KRUG, T. Utilização de dados MODIS para a detecção de queimadas na Amazônia. **Acta Amazonica**, vol. 38, n. 1, p. 77–84, 2008. DOI: 10.1590/S0044-59672008000100009.
- RAMO, R.; CHUVIECO, E. Developing a Random Forest algorithm for MODIS global burned area classification. **Remote Sensing**, vol. 9, n. 11, p.1193-1215, 2017. DOI:10.3390/rs9111193.
- ROUSE, J. W.; HASS, R. H.; SCHELL, J.A.; DEERING, D.W. Monitoring vegetation systems in the great plains with ERTS. **Proceeding of Third Earth Resources Technology Satellite (ERTS) Symposium**, vol. 1, p. 309–317, 1973.
- SHIMABUKURO, Y. E.; DUARTE, V.; ARAI, E.; FREITAS, R. M.; LIMA, A.; VALERIANO, D. M.; BROWN, I. F.; MALDONADO, M. L. R. Fraction images derived from Terra Modis data for mapping burnt areas in Brazilian Amazonia. **International Journal of Remote Sensing**, vol. 30, n. 6, p. 1537–1546, 2009. DOI: 10.1080/01431160802509058.
- SHIMABUKURO, Y. E.; MIETTINEN, J.; BEUCHLE, RENE; GRECCHI, R. C.; SIMONETTI, D.; ACHARD, F. Estimating burned area in Mato Grosso, Brazil, using an object-based classification method on a systematic sample of medium resolution satellite images. **IEEE Journal of Selected Topics in Applied Earth Observations and Remote Sensing**, vol. 8, n. 9, p. 4502–4508, 2015. DOI: 10.1109/JSTARS.2015.2464097.
- SHIMABUKURO, Y. E.; SMITH, J. A. The least-squares mixing models to generate fraction images derived from remote sensing multispectral data. **IEEE Transactions on Geoscience and Remote Sensing**, vol. 29, n. 1, p. 16–20, 1991. DOI: 10.1109/36.103288.
- SMITH, M. S.; DRAKE, N.; WOOSTER, M J; HUDAK, T.; HOLDEN, Z.; GIBBONS, C J. Production of Landsat ETM+ reference imagery of burned areas within Southern African savannahs: comparison of methods and application to MODIS. **International Journal of Remote Sensing**, vol. 28, n. 12, p. 2753–2775, 2007. DOI: 10.1080/01431160600954704.
- TRIGG, S.; FLASSE, S. An evaluation of different bi-spectral spaces for discriminating burned shrub-savannah. **International Journal of Remote Sensing**, vol. 22, n. 13, p. 2641–2647, 2001. DOI: 10.1080/01431160110053185.
- VAN DER WERF, G. R.; RANDERSON, J. T.; GIGLIO, L.; COLLATZ, G. J.; MU, M.; KASIBHATLA, P. S.; MORTON, D. C.; DEFRIES, R. S.; JIN, Y.; VAN LEEUWEN, T. T. Global fire emissions and the contribution of deforestation, savanna, forest, agricultural, and peat fires (1997-2009). **Atmospheric Chemistry and Physics**, vol. 10, n. 23, p. 11707–11735, 2010. DOI: 10.5194/acp-10-11707-2010.
- VEDOVATO, L. B.; JACON, A. D.; PESSÔA, A. C. M.; LIMA, A.; ARAGÃO, L. E. O. C. Detection of burned forests in Amazonia using the Normalized Burn Ratio (NBR) and Linear Spectral Mixture Model

from Landsat 8 images. In: SIMPÓSIO BRASILEIRO DE SENSORIAMENTO REMOTO, 17, 2015, João Pessoa. **Anais...** João Pessoa: INPE, 2015. p. 2984–2991.

VERMOTE, E.; JUSTICE, C.; CLAVERIE, M.; FRANCH, B. Preliminary analysis of the performance of the Landsat 8/OLI land surface reflectance product. **Remote Sensing of Environment**, v. 185, p. 46–56, 2016. DOI: 10.1016/j.rse.2016.04.008.

WULDER, M. A.; MASEK, J. G.; COHEN, W. B.; LOVELAND, T. R.; WOODCOCK, C. E. Opening the archive: How free data has enabled the science and monitoring promise of Landsat. **Remote Sensing of Environment**, vol. 122, p. 2–10, 2012. DOI: 10.1016/j.rse.2012.01.010.

YAN, L.; ROY, D. P.; ZHANG, H.; LI, J.; HUANG, H. An automated approach for sub-pixel registration of Landsat-8 Operational Land Imager (OLI) and Sentinel-2 Multi Spectral Instrument (MSI) imagery. **Remote Sensing**, vol. 8, n. 6, p. 520-543, 2016. DOI: 10.3390/rs8060520.

ZHU, Z.; WOODCOCK, C. E. Object-based cloud and cloud shadow detection in Landsat imagery. **Remote Sensing of Environment**, vol. 118, p. 83-94, 2012. DOI: 10.1016/j.rse.2011.10.028.

ZHU, Z.; WANG, S.; WOODCOCK, C. E. 2015. Improvement and expansion of the Fmask algorithm: cloud, cloud shadow, and snow detection for Landsats 4–7, 8, and Sentinel 2 images. **Remote Sensing of Environment**, vol. 159, p. 269-277, 2015. DOI: 10.1016/j.rse.2014.12.014.

Main author biography



Thales Vaz Penha was born in Rio de Janeiro, Brazil. He holds his BSc in Geography from the Fluminense Federal University (UFF) and his MSc in Remote Sensing from the Brazilian Institute for Space Research (INPE). Having previously worked as a research assistant and GIS consultant, he is currently a Ph.D. candidate in Physical Geography from the University of São Paulo. His research interests include the use of GIS and Remote Sensing applied to Amazonian vegetation disturbs mapping and the analysis of fires and forest fires impacts in people's vulnerability, considering the climate change perspective.



Esta obra está licenciada com uma Licença [Creative Commons Atribuição 4.0 Internacional](https://creativecommons.org/licenses/by/4.0/) – CC BY. Esta licença permite que outros distribuam, remixem, adaptem e criem a partir do seu trabalho, mesmo para fins comerciais, desde que lhe atribuam o devido crédito pela criação original.